IEEE Access
Multidisciplinary | Rapid Review | Open Access Journal

Received December 8, 2020, accepted January 10, 2021, date of publication January 19, 2021, date of current version January 28, 2021.

Digital Object Identifier 10.1109/ACCESS.2021.3052864

Vessel Recognition in Induction Heating Appliances–A Deep-Learning Approach

JORGE VILLA[1], (Member, IEEE), DENIS NAVARRO[1], ALBERTO DOMINGUEZ[2], JOSE I. ARTIGAS[1], AND LUIS A. BARRAGAN[1]

[1]Department of Electronic Engineering and Communications, I3A, University of Zaragoza, 50018 Zaragoza, Spain
[2]Bosch and Siemens Home Appliances Group, Department of Induction Technology of BSH Electrodomesticos, 50016 Zaragoza, Spain

Corresponding author: Jorge Villa (jvillal@unizar.es)

This work was supported in part by the Spanish MICINN under Project PID2019-103939RB-I00, in part by the Spanish MICINN and AEI under Project RTC-2017-5965-6 and Grant PTQ-17-09045, in part by the EU through FEDER Program, in part by the DGA-FSE, and in part by the BSH Home Appliances Group.

ABSTRACT The selection of a vessel by an induction-hob user has a significant impact on the performance of the appliance. Due to the induction heating physical phenomena, there exist many factors that modify the equivalent impedance of induction hobs and, consequently, the operational conditions of the inverter. In particular, the type of vessel, which is a sole decision of the user, strongly affects these parameters. Besides, the ferromagnetic properties of the different materials the vessels are made with, vary differently with the excitation level, and given that most of the domestic induction hobs are based on an ac-bus voltage arrangement, the excitation level continuously varies. The algorithm proposed in this work takes advantage of this fact to identify the equivalent impedance of the load and recognize the pot. This is accomplished through a phase-sensitive detector that was already proposed in the literature and the application of deep learning. Different convolutional neural networks are tested on an augmented experimental-based dataset and the proposed algorithm is implemented in an experimental prototype with a system-on-chip. The proposed implementation is presented as an effective and accurate method to characterize and discriminate between different pots that could enable further functionalities in new generations of induction hobs.

INDEX TERMS Convolutional neural network, home appliances, induction heating, neural network applications, system-on-chip (SoC).

I. INTRODUCTION

Induction heating is a contact-less heating method that has been widely used in many applications [1]–[3]. The development of semiconductor devices for power electronics and the contact-less nature of this heating technology makes it preferred over other heating methods due to its higher efficiency. In the domestic induction heating (DIH) case, its main advantage compared to the resistive cooktops is that while in the last ones the hottest component is the resistor, in the former, the hottest element is the bottom part of the pot. Logically, this offers higher efficiencies while a colder cooking surface leads to a safer, easier-to-clean and more durable home appliance [4].

However, given the characteristics of the equivalent load, the control of an induction hob is more complicated than the one of a resistive cooktop. The alternating magnetic field that heats the bottom of the pot due to induced current losses and magnetic hysteresis [5], [6] is usually generated with a half-bridge series resonant inverter. The equivalent impedance of the load is modeled as a resistance, R, connected in series with an inductance, L, [7], and the resonant behavior is achieved by adding a resonant capacitor, C_r, in series with the load. To feed the inverter, the grid voltage, v_{grid}, is full-wave rectified and filtered with a bus capacitor, leading to a high-rippled voltage called bus voltage, v_B, whose fundamental frequency is twice the one of v_{grid}. Given the low-cost context of DIH, the switching frequency, f_{sw}, which spans from 30 to 75 kHz, is usually generated through insulated gate bipolar transistors (IGBTs). The lower limit of f_{sw} is imposed by the maximum frequency of human hearing, which is roughly established at 20 kHz, while the upper limit of the switching frequency is set to reduce the switching losses. Additionally, in the input of the home appliance a filter is placed to improve

The associate editor coordinating the review of this manuscript and approving it for publication was Fanbiao Li.

the electromagnetic compatibility (EMC) with the grid. This filter is mainly designed to comply with the standards that limit the emissions of radio-frequency disturbances in the frequency range from 9 kHz to 30 MHz.

One of the drawbacks but also challenges of DIH is that the equivalent load varies with many parameters such as the switching frequency, the excitation level, the characteristics of the pot (material, size, temperature), the misalignment and distance between the inductor and the pot, etc. Besides, many of these parameters depend exclusively on the user.

Such variation of the load forces the control system to change and monitor the operational conditions of the inverter to guarantee the maximum performance and a safe operation of the electronics. For this reason, much effort has been focused on identifying the equivalent load and so is reflected in the literature [8]–[15]. While these methods try to capture the equivalent impedance of the load, they are not able to classify different pots and discriminate between them, i.e., if a user has ten different pots, to be able to recognize which one of those ten pots is used at a time. Although some years ago this could be seen as an idealistic functionality, with the increasing computational capacity of new system-on-chips (SoCs) and processors and the development of the internet-of-things (many induction home appliances are connected to the internet nowadays) these functions are getting closer and closer to a real implementation.

The recognition of the pot could improve the user experience by enabling further functionalities such as the detection of commonly used pots, a better detection of the suitability of a pot for induction heating, the warning of a misaligned pot, the control of the use and ageing of a specific pot, etc. Moreover, more accurate thermal models could be achieved [16] which would ultimately lead to a better estimation of the temperature and the cooking process. Besides, the appliance could use information from previous cookings such as an approximation of the power-switching frequency transfer function, which pots are used for which types of cooking processes and for how long, etc. This information could simplify the algorithms that distribute the power between different inductors, lead to faster responses to a change in the power target and enable advanced features in new generations of home appliances, e.g.: imagine placing a coffee pot on the cooking surface and the appliance automatically recognizing that this is your coffee pot and that you are going to make a coffee, just because you have done so in previous days.

However, to obtain this information, an accurate identification that could serve as a fingerprint for each pot would be certainly helpful. In [17], the equivalent impedance of the load is analyzed from the perspective of the electromagnetic properties of the material of the pot. Apart from other parameters, the equivalent impedance depends on the electrical conductivity and magnetic permeability of the material. Besides, the magnetic permeability varies with the excitation level and, fortunately, different materials respond differently to that variation of the excitation level. Moreover, given the high ripple of the bus voltage, the excitation level applied to the pot varies continuously even if a constant switching frequency is applied.

The methods proposed in [8]–[14] whether calculate a single and averaged value of the equivalent impedance per bus cycle (or for many switching cycles) or base their work on a dc-bus voltage arrangement, meaning that they can only extract information about the average inductiveness or resistiveness of the loads. Nonetheless, no underlying information about the materials, extracted from the variation of their electromagnetic properties due to the variation of the excitation level, can be obtained. On the contrary, in [15] this information is provided thanks to an algorithm that tracks the variation of the equivalent impedance with the excitation level along the entire bus period. However, although the impedance difference between pots that are made of different materials is shown, no automatic recognition of pots is proposed.

On the other hand, deep learning has also been used for the identification of certain parameters in induction hobs. For instance, in [18] a convolutional neural network based on the average power, rms current and quality factor of the load is proposed to estimate the overlap area between the pot and the inductors (a flexible induction hob is used, where many small inductors lead to a flexible cooking area). In [19] the authors calculate the power factor and the absolute value of the impedance, $|\boldsymbol{Z}|$, for the first four harmonics of the switching frequency and apply a neural network to estimate the size of the vessel placed above the inductor. In this case, the algorithm is implemented in a simpler induction hob with a single inductor and a single-switch inverter.

Likewise, in [20] a method to classify different types of pots (or materials) is proposed. They use the same information as in [19], but they make sure the impedance $|\boldsymbol{Z}|$ and the power factor are calculated at a bus voltage of 100 V. Then, different machine learning algorithms are tested and proposed. However, although the authors are aware of the variation of the equivalent impedance with the excitation level (this is why they make sure the identification is applied at a constant bus voltage), they do not take advantage of this phenomenon to extract more information about the materials.

In this paper, a method to identify the pot that is placed above the inductor is proposed. The inductor is used as a smart sensor so that, compared to a traditional induction hob, no additional hardware is required. Furthermore, no limitations neither on the switching frequency (as long as it is constant during the entire bus period) nor on the bus voltage are imposed. The identification of the equivalent impedance is obtained with the algorithm suggested in [15], and the recognition of the vessel is achieved by means of a convolutional neural network (CNN) whose only inputs are two vectors which contain the values of R and L during a bus period. The neural network is trained and validated offline, and finally implemented into a prototype with system-on-chip (SoC).

This paper is organized as follows. In Section II the method to identify the equivalent impedance as well as the data acquisition process are briefly explained. The proposed neural network, the data augmentation and training processes and

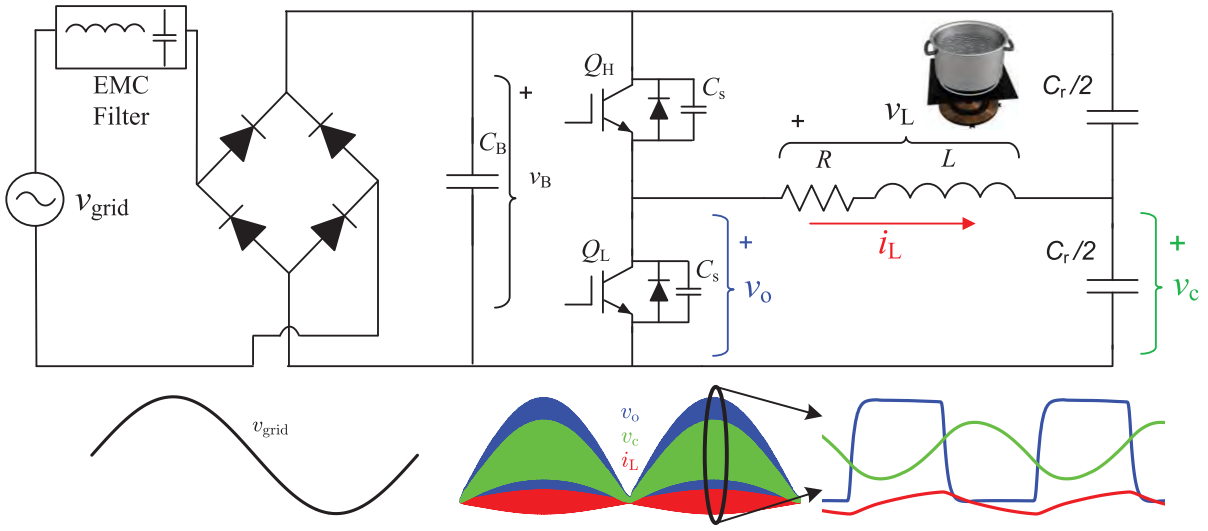

FIGURE 1. Simplified schematic of the induction hob and its main waveforms. v_{grid} is rectified and the small bus capacitor leads to a very high rippled bus voltage which directly feeds the inverter. Switches Q_H and Q_L generate the alternating current and snubber capacitors are included to reduce the switching losses.

the main results are described in Section III. Then, the implementation of the whole system in a prototype is presented in Section IV. Finally, Section V concludes this article.

II. IDENTIFICATION METHOD AND EXPERIMENTAL DATA ACQUISITION

In Fig. 1 a simplified schematic of the half-bridge series resonant inverter is shown. The identification of the equivalent impedance of the load is based on the method proposed in [15] because it is the one (among [8]–[15]) that extracts more information about the load: it provides the values of the $R-L$ equivalent impedance and its variation with the excitation level, what intrinsically shows how the ferromagnetic properties of the materials of the pots vary.

To accurately obtain the equivalent impedance with this method, it is necessary to measure the voltage drop of the load, v_L, and the current that flows through the inductor, i_L. The voltage v_L is indirectly calculated from the subtraction of the output voltage of the inverter, v_o, and the resonant capacitor voltage, v_c, ($v_L = v_o - v_c$) and i_L is usually measured with a current transformer. The identification method is based on a phase-sensitive detector (PSD), which generates the sinusoidal signals that are synchronized with the inverter signals. After some operations and low-pass filtering, the cosine and sine first-harmonic components of v_L and i_L, which are denoted as $V_{L,c}$, $V_{L,s}$, $I_{L,c}$, and $I_{L,s}$ (subindex "1h" referring to first harmonic is dropped out for notation simplicity), are obtained and, with these values, and the angular switching frequency, ω_{sw}, the first-harmonic equivalent impedance is obtained as:

$$R \approx R_{1h} = \frac{V_{L,c}I_{L,c} + V_{L,s}I_{L,s}}{I_{L,c}^2 + I_{L,s}^2}$$
$$L \approx L_{1h} = \frac{V_{L,c}I_{L,s} - V_{L,s}I_{L,c}}{\omega_{sw}(I_{L,c}^2 + I_{L,s}^2)}, \quad (1)$$

where it is assumed that the phasors of the load voltage and the current are given by $\boldsymbol{V}_{L,1h} = V_{L,c} - jV_{L,s}$ and $\boldsymbol{I}_{L,1h} = I_{L,c} - jI_{L,s}$, respectively. For more specific information about this identification method, one may refer to [15].

For an appropriate study of the presented problem, a large experimental dataset that includes a wide variety of pots is required and, to record it, an experimental prototype with an automatic data acquisition functionality would be mandatory. For this reason, the data acquisition in the experimental prototype was fully automated. To obtain the dataset the researcher only has to place a pot filled with water on the inductor and launch the automatic process that is explained in Algorithm 1, which must be repeated as many times as the number of pots to be identified. This was accomplished thanks to a Direct Memory Access (DMA) controller, which, for every switching frequency, transfers the values of $V_{L,c}$, $V_{L,s}$, $I_{L,c}$, $I_{L,s}$ and ω_{sw} during a bus period to the Double Data Rate Synchronous Dynamic Random-Access Memory (DDR-SDRAM) available in the prototype (more information will be provided in Section IV). This transaction is synchronized with the zero-crossing of the grid voltage and, for a grid period of 50 Hz, a total of 868 values (per switching frequency) of the mentioned variables are saved. Additionally, thanks to this implementation it would be possible to create a repository to storage a track record of old and new vessels that are launched onto the market.

Then, the impedance values are calculated offline with (1), obtaining 868 values of R and L for every switching frequency. Since for the current implementation of Algorithm 1, $\Delta f_{sw} = 500$ Hz, $f_{sw,max} = 75$ kHz and the maximum power for most of the pots is reached at $f_{sw,@maxPower}$ below 40 kHz, at least 70 curves of $R-L$ are recorded; that is more than 60 thousand values of R and L for every pot. The whole process shown in Algorithm 1 takes less than two seconds

Algorithm 1 Automatic Data Acquisition

$f_{sw} \leftarrow f_{sw,@maxPower}$
while $f_{sw} \leq f_{sw,max}$ **do**
  Launch DMA transaction (save ω_{sw} and vectors $V_{L,c}$, $V_{L,s}$, $I_{L,c}$ and $I_{L,s}$)
  wait until DMA transaction is completed
  $f_{sw} \leftarrow f_{sw} + \Delta f_{sw}$
end while
Send data to laptop

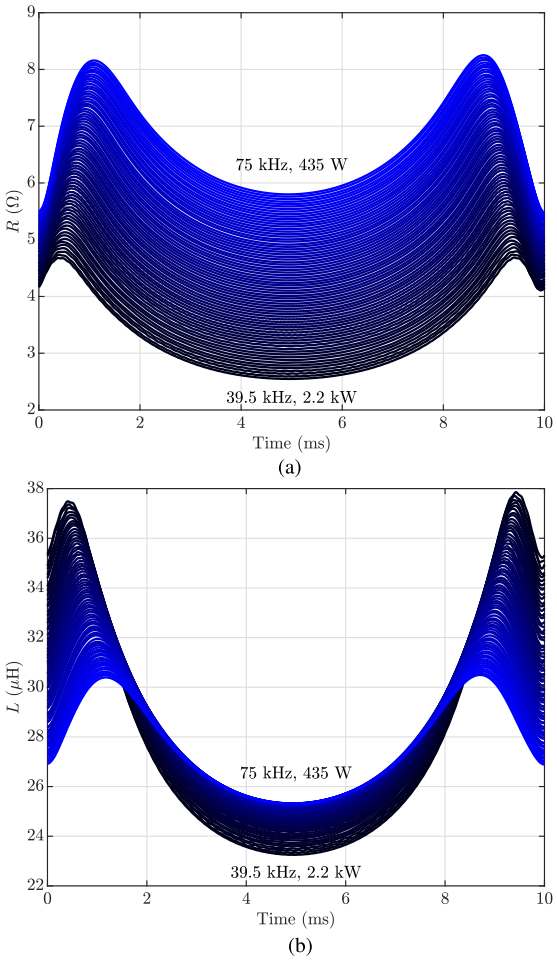

FIGURE 2. Result of the automatic identification algorithm for an enameled pot. Every curve corresponds to the $R - L$ values during a bus period at a specific switching frequency. The crest of the bus period is at 5 ms. (a) Resistance. (b) Inductance.

per pot. An example of the data obtained for one pot is shown in Fig. 2.

III. THE NEURAL NETWORK

Deep learning is a widespread technique that has been increasingly used during the last years. This is motivated by its ability to solve very complicated and non-linear problems by learning complex patterns from large datasets [21], [22]. Moreover, unlike other traditional methods, it does not require neither the use of extremely complex mathematical expressions nor a deep expertise in the physics behind the problem to be solved.

There exist many types of neural networks; one of them, known as fully connected neural network, connect each neuron in a layer to all the neurons in the next layer, what exponentially increases its size and computational complexity with the network depth. On the other hand, convolutional neural networks take advantage of hierarchical patterns in data to combine that information into smaller and simpler patterns that are successively reduced in the following layers. This reduces the computational complexity and the number of coefficients to be learned by the network, which are two crucial aspects for a feasible real-time implementation in an embedded system (limited memory and limited computational capacity). Furthermore, convolutional neural networks have been successfully applied to a wide variety of applications such as image recognition for industry [23] and medicine [24], speech recognition [25], fault diagnosis in mechanical components [26], etc.

A CNN is usually made of convolutional layers and pooling layers. In the convolutional layer, the input, in our case the $R - L$ vectors, is convolved with a kernel or filter which extracts the features. Then, an activation function is applied to obtain nonlinear transformations. The next type of layers, the pooling layers, reduces the dimension of the data by extracting the dominant features. This process is applied as many times as the number of levels (depth) the network has. Finally, a fully connected layer is applied to the result of the last layer, which computes the class scores and outputs the final result.

Apart from the low computational complexity of CNNs, there is another reason to choose this type of networks for this application: it takes into account the local connectivity of the data thanks to the connection between neurons (a neuron in one layer is connected to some regions of the previous layer through the kernel or the filter bank). This local connectivity and neighboring relationship is also one of the reasons why this type of neural networks performs very well in computer vision applications [23], [24].

In this work, the activation function which provides the nonlinear transformation is the rectified linear unit (ReLU) and it is defined as:

$$\text{ReLU} : f(x) = \max\{0, x\}, \tag{2}$$

where x is the output from the previous convolutional layer.

A. DATA AUGMENTATION AND TRAINING

The experimental data was obtained for 19 different pots (different diameters, materials, manufacturers and brands). These pots where placed on the inductor while trying to align the inductor and the pot as good as possible and making sure the water was boiling when the automatic data acquisition was launched (just for standardizing the acquisition of data). Besides, for 4 of these 19 pots additional experimental data was captured at different temperatures (from ambient temperature to 100 °C) and at different positions (pot aligned

with the inductor and with a radial horizontal displacement inductor-pot of 4 and 8 centimeters).

The purpose of this set of measurements is to test if the convolutional neural network is able, apart from discriminating between different pots, to detect if a pot is not properly aligned with the inductor (no matter the temperature) or, what is equivalent from the point of view of the load, if a too small pot is used. This is an important issue in induction hobs because when a pot is not well aligned with the inductor the resistance decreases and, to supply the same power, the current i_L would reach such levels that are not withstood by the power electronic devices. It is worth mentioning that a traditional resistive cooktop provides a constant power and if the pot is smaller than the resistance, the heat supplied to the pot is automatically reduced because of the smaller area of interaction. However, induction hobs need a more sophisticated control that is able to reduce the power when these smaller pots are detected. Otherwise, the user would perceive that smaller (or misaligned) pots are overheated.

To sum up, taking into account the 19 different pots and the additional measurements for 4 of them, that gives us a total of 27 different tags or identifiers (because of the misalignments) to be recognized by the neural network. A total of 300 sweeps were performed, and considering that in every sweep approximately 70 switching frequencies are analyzed, that gives us a total of 20790 curves of $R - L$ for the whole set of pots.

Since during the training process of the neural network, the coefficients of the kernel have to be adjusted, large dataset are required, so that the probability of over-fitting is reduced. The need for a large and diverse dataset is in fact one of the challenges for the success of neural networks. Although 20790 curves might be seen as a decently large dataset, data augmentation is carried out in this work. This is a commonly used technique, which has already been used in other applications [27], [28], when the amount of experimental data is not considered large or diverse enough.

Furthermore, in the real application small deviations and noise could appear in the identification, and this is something that should be considered in the training stage of the network. Thus, every $R - L$ vector is multiplied by a random factor in the range [0.9, 1.1], then, a random offset in the range [0.9, 1.1] of the average value of the vector is added, and a random noise of $\pm 1\%$ is added to every sample in the vector. Furthermore, considering that the zero-crossing synchronization of v_{grid} in the real hob might not be ideal, a circular shift of a random number of samples in the range [-10, 10] is applied to the vectors. An example of the result of this process is shown in Fig 3. This process is applied many times to the data saved for every pot until the error rate obtained for the training dataset equals the one of the testing dataset. Moreover, the data augmentation algorithm makes sure that the same number of curves are generated for every pot, even if in the experimental data acquisition this condition did not hold. This assures that the recognition of all the pots will be similarly weighted during the optimization of the training process. The final dataset is divided into two equally sized sets of 653400 curves.

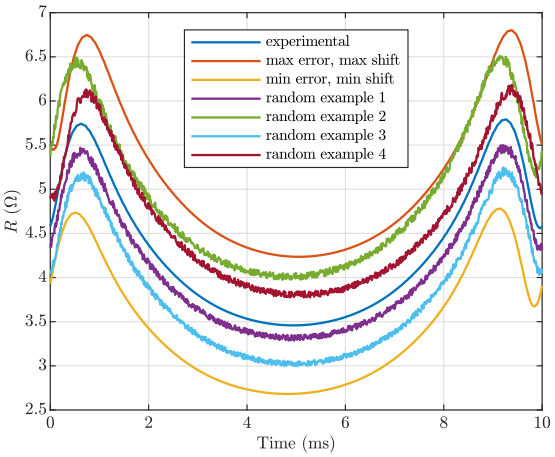

FIGURE 3. Example of data augmentation process (only resistance is shown).

B. THE PROPOSED NEURAL NETWORK

Before implementing the CNN into the prototype, several networks were trained and tested offline. To do so, an exhaustive study changing the number of convolutional layers (#C), the stride, the kernel (K) size, the number of kernels (#K) and the size of the pooling layers was performed. Given that the final goal is the implementation in an embedded device, the number of coefficients was limited to a maximum value of approximately 20k. The number of filters, $n_{fil,1}$, and kernel size, $k_{size,1}$, for the first convolutional layer were obtained as:

$$n_{fil,1} = 2\#\mathrm{K} \qquad k_{size,1} = \mathrm{size(K)} \tag{3}$$

Likewise, for the second convolutional layer, $n_{fil,2}$ and $k_{size,2}$ were calculated as:

$$n_{fil,2} = 2\#\mathrm{K}^2 \quad k_{size,2} = \lfloor \mathrm{size(K)/Stride} \rfloor, \tag{4}$$

Convolutional neural networks with one and two convolutional layers were considered because the test accuracy obtained with two layers was already great. The training and testing were performed with TensorFlow and Matlab using an NVIDIA GTX1085Ti GPU. The results of the parametric study are shown in Table 1, where the number of coefficients (#Coeff.), the required multiply-accumulate operations (#MAC) and the errors are given for each tested network. Note that in CNNs with a single convolutional layer no pooling layers are used.

Apart from CNNs, long short-term memory (LSTM) and gated recurrent unit (GRU) networks were also tested, but their results are not discussed in this article because they underperformed most of the analyzed CNNs.

Finally, the CNN that offered the lowest error in the test (see Table 1) was selected as the best candidate for the real-time implementation. It is a CNN with two convolutional

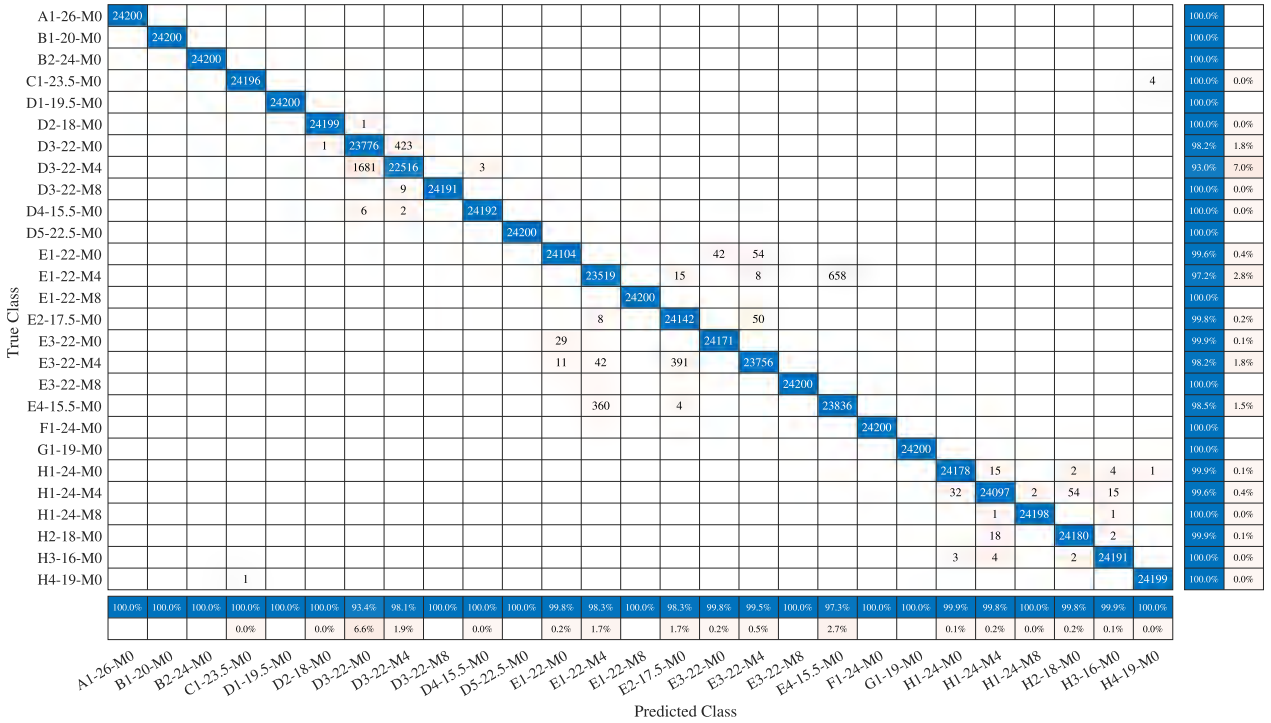

FIGURE 4. Confusion matrix of the selected two-layer CNN (number 17 in Table 1). The first letter in the tag is the identifier of the brand/type of the pot (whether it is enameled, sandwich, multilayer, etc.), the next number identifies different pots of a given brand/type, the number between the hyphens is the diameter of the pot in centimeters, and the number after the "M" letter is the radial misalignment with respect to the inductor in centimeters.

TABLE 1. Parametric study of CNNs.

#	#C	Stride	#K	Size(K)	Size(pool)	#Coeff.	#MAC	Error (%)
1	1	18	15	66	-	20247	107325	1.2597
2		14	12	78	-	20379	125172	1.2849
3		18	15	56	-	20352	95910	1.4450
4		14	12	68	-	20463	113448	1.4678
5		14	12	58	-	20223	99528	1.4713
6		10	9	70	-	20736	120240	1.6187
7		10	9	40	-	20925	79929	2.0456
8		18	15	36	-	20157	69795	2.0973
9		14	12	28	-	20475	60756	2.5176
10		6	5	42	-	19082	76590	2.8187
11		10	9	20	-	21051	51255	3.3996
12		2	2	54	-	22277	110160	5.1951
13		2	2	74	-	21817	139300	5.9634
14		2	2	24	-	22967	63450	6.2004
15		6	5	12	-	19457	36465	7.2309
16		2	2	4	-	23427	30310	14.7650
17	2	4	6	80	4	21463	173832	0.7819
18		4	5	40	2	21387	152860	0.8939
19		8	6	80	3	10879	43728	1.3504
20		4	6	40	4	12743	115592	2.7315
21		5	8	40	4	20123	131456	3.0408
22		5	6	40	3	12959	88256	3.6784
23		5	5	20	2	12947	51620	5.2095

layers whose detailed structure, the size of the data between layers and the number of parameters of each kernel are summarized in Table 2.

The confusion matrix of the selected network is shown in Fig. 4. It is worth mentioning that for the original data

TABLE 2. Internal structure of the selected two-layer CNN.

Layer type	Output Size	#Param
SeparableConv1D	198x12	196
MaxPooling1D	49x12	0
ReLU	49x12	0
Conv1D	8x72	17352
MaxPooling1D	2x72	0
ReLU	2x72	0
Fully connected	27	3915
Total coeff.		21,463

(without data augmentation) the confusion matrix showed no errors. In Fig. 4 it can be observed that the CNN is able to recognize the pot most of the times and it rarely mistakes pots of different brands or types. Some mistakes are observed when the CNN tries to detect a misalignment (see D3-22-M0 and D3-22-M4) or when two different pots of the same brand/type with the same diameter are aligned with the inductor (see E1-22-M0 and E3-22-M0).

Moreover, it can be noticed that for a given type of pot, let's say type "E", if a big pot is misaligned 4 cm (E3-22-M4), the CNN sometimes mistakes it for an aligned but smaller pot (E2-17.5-M0). In fact, this was an expected behavior because from the point of view of the load, those situations might be seen as equivalent.

IV. IMPLEMENTATION

The experimental prototype is made of some parts of a commercial induction hob and two printed circuit boards

FIGURE 5. Experimental prototype.

(PCBs) that were designed for research purposes. One of the PCBs mounts the power electronics circuitry and the other one, which can be connected to the former, mounts the conditioning and acquisition circuits. Besides, the second PCB is compatible with the carrier board TE0703 from Trenz Electronics, which is connected to the system-on-module (SoM) TE0720 (also from Trenz Electronics) which, in turn, includes the system-on-chip Zynq-7020. This SoC includes in a single chip the field-programmable gate array (FPGA) fabric and a dual core ARM Cortex-A9 processor. Besides, the SoM also includes a 1 GB DDR-SDRAM.

The acquisition of the electrical signals v_o, v_c, i_L and v_{grid} (this last variable is used for the synchronization with the zero-crossing of the grid voltage) is accomplished through 12-bit LTC-2315-12 analog-to-digital converters (ADCs) whose sampling frequency is set at 2.78 Msps. These ADCs are controlled through a serial peripheral interface (SPI) protocol.

The modulator that controls the IGBTs, the identification of the load [15], the control of the ADCs and the controller of the DMA transactions are implemented on the FPGA fabric whose clock frequency is set at 100 MHz. The signals $V_{L,c}$, $V_{L,s}$, $I_{L,c}$, $I_{L,s}$ and ω_{sw} are sent to the DMA controller through the Advanced eXtensible Interface 4 (AXI4)-Stream protocol. Finally, the DMA controller, which is configured in stream to memory-map mode, writes the data in the DDR-SDRAM whenever the ARM (core 1) processor requests it.

At the same time the ARM (core 0), which runs the operating system Petalinux, is in charge of the communication with a graphical user interface (GUI) programmed in Matlab and running in a laptop. This communication is established over Ethernet through a TCP/IP protocol and was of great importance for the automatic data acquisition explained in Section II.

The convolutional neural network is implemented in floating point (single precision) in the core 1 of the ARM processor. To do so, an interrupt is generated with one of the triple time counters (TTCs), whose interrupt handler launches a DMA transaction which saves the vectors $V_{L,c}$, $V_{L,s}$, $I_{L,c}$, $I_{L,s}$ and ω_{sw} of a bus period in the DDR-SDRAM. When the transaction finishes, an interrupt is generated, and after computing (1) for each of the 868 samples, the CNN is executed. This process is executed 10 times per second, leaving time for the ARM (core 1) to run other tasks such as control of power, monitoring of variables, etc. The clock frequency of the ARM is 667 MHz. It is worth mentioning that in the final application, depending on the requirements of the induction hob and the features of its SoC, it might not be necessary to recognize the pot continuously or at least not at such a fast rate.

The entire code, once programmed in C, requires 130 kB of memory including the more than 85 kB of coefficients. The execution of the convolutional neural network together with the calculation of the $R - L$ values (1) takes about 2.55 ms in the ARM. It is worth noting that the CNN is executed only once every 100 ms. A simplified block diagram of the system is shown in Fig 6.

A video is attached with this work where the performance of the real-time implementation in the prototype is shown. In this video, different pots at different misalignments are

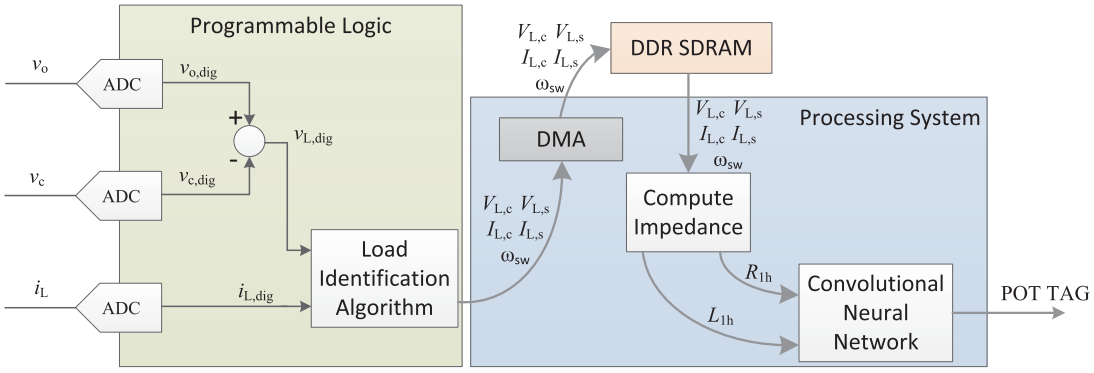

FIGURE 6. Simplified block diagram of the system. Subindex "dig" refers to digital and has only been added to differentiate between analog and digital signals.

placed on the inductor while the SoC executes the proposed algorithm and prints the tag of the predicted pot through a terminal.

V. CONCLUSION

Deep learning has been evolving during the last years due to the continuously increasing computational capacity of new technologies and its amazing ability to learn complex patterns from large datasets.

In this work, a convolutional neural network is applied to recognize the pot that is heated in a domestic induction hob. The input data to the neural network are two vectors of 868 values each which contain the variation of the equivalent resistance and inductance of the load during a bus period.

To train the neural network, the equivalent impedance of several pots was identified during a bus cycle for different switching frequencies, temperatures and misalignments. Through data augmentation, a large dataset was obtained, with which the neural network was trained. Several types of neural networks were tested offline by varying the number of layers, the stride, the filter size and the number of filters of each layer. The results obtained during the testing process show that the proposed CNN is able to successfully recognize the pots with an average error rate of 0.7819%. Besides, the experimental results show that the proposed solution is also able to estimate if, and how much, a pot is misaligned with the inductor even when the equivalent impedance is identified at different pot temperatures.

Moreover, with the proposed method, the inductor is used as a smart-sensor, so that no extra-hardware is required, preserving the low-cost nature of DIH and taking advantage of the increasingly higher computational complexity available in embedded systems.

Finally, the proposed CNN was implemented in an experimental prototype to show its real-time performance and the feasibility of its inclusion in a real hob. This is the first implementation of a pot identifier based on convolutional neural networks and the information of the variation of the equivalent impedance with the excitation level, which will help broadening the research and development areas in domestic induction heating and will enable new functionalities in future generations of induction hobs.

REFERENCES

[1] N. A. Ahmed, "High-frequency soft-switching AC conversion circuit with dual-mode PWM/PDM control strategy for high-power IH applications," *IEEE Trans. Ind. Electron.*, vol. 58, no. 4, pp. 1440–1448, Apr. 2011.

[2] V. Esteve, J. Jordan, E. Sanchis-Kilders, E. J. Dede, E. Maset, J. B. Ejea, and A. Ferreres, "Enhanced pulse-density-modulated power control for high-frequency induction heating inverters," *IEEE Trans. Ind. Electron.*, vol. 62, no. 11, pp. 6905–6914, Nov. 2015.

[3] J. Acero, J. Burdío, L. Barragán, D. Navarro, R. Alonso, J. García, F. Monterde, P. Hernández, and S. L. I. Garde, "Domestic induction appliances," *IEEE Ind. Appl. Mag.*, vol. 16, no. 2, pp. 39–47, Mar. 2010.

[4] O. Lucia, J. Acero, C. Carretero, and J. M. Burdio, "Induction heating appliances: Toward more flexible cooking surfaces," *IEEE Ind. Electron. Mag.*, vol. 7, no. 3, pp. 35–47, Sep. 2013.

[5] J. Acero, C. Carretero, R. Alonso, and J. M. Burdio, "Quantitative evaluation of induction efficiency in domestic induction heating applications," *IEEE Trans. Magn.*, vol. 49, no. 4, pp. 1382–1389, Apr. 2013.

[6] H. Kurose, D. Miyagi, N. Takahashi, N. Uchida, and K. Kawanaka, "3-D eddy current analysis of induction heating apparatus considering heat emission, heat conduction, and temperature dependence of magnetic characteristics," *IEEE Trans. Magn.*, vol. 45, no. 3, pp. 1847–1850, Mar. 2009.

[7] J. Acero, O. Lucia, I. Millan, L. A. Barragan, J.-M. Burdio, and R. Alonso, "Identification of the material properties used in domestic induction heating appliances for system-level simulation and design purposes," in *Proc. 25th Annu. IEEE Appl. Power Electron. Conf. Expo. (APEC)*, Feb. 2010, pp. 439–443.

[8] B. A. Nguyen, Q. D. Phan, D. M. Nguyen, K. L. Nguyen, O. Durrieu, and P. Maussion, "Parameter identification method for a three-phase induction heating system," *IEEE Trans. Ind. Appl.*, vol. 51, no. 6, pp. 4853–4860, Nov. 2015.

[9] A. Dominguez, A. Otin, I. Urriza, L. A. Barragan, D. Navarro, and J. I. Artigas, "Load identification of domestic induction heating based on particle swarm optimization," in *Proc. IEEE 15th Workshop Control Modeling Power Electron. (COMPEL)*, Jun. 2014, pp. 1–6.

[10] O. Jimenez, L. A. Barragan, I. Urriza, O. Lucia, D. Navarro, and J. I. Artigas, "FPGA-based real-time harmonic impedance measurement of series resonant loads by using lock-in algorithm," in *Proc. 37th Annu. Conf. IEEE Ind. Electron. Soc. (IECON)*, Nov. 2011, pp. 2808–2813.

[11] O. Jimenez, O. Lucia, I. Urriza, L. A. Barragan, and D. Navarro, "Analysis and implementation of FPGA-based online parametric identification algorithms for resonant power converters," *IEEE Trans. Ind. Informat.*, vol. 10, no. 2, pp. 1144–1153, May 2014.

[12] V. T. Kilic, E. Unal, N. Yilmaz, and H. V. Demir, "All-surface induction heating with high efficiency and space invariance enabled by arraying squircle coils in square lattice," *IEEE Trans. Consum. Electron.*, vol. 64, no. 3, pp. 339–347, Aug. 2018.

[13] D. Puyal, C. Bernal, J. M. Burdio, J. Acero, and I. Millan, "Versatile high-frequency inverter module for large-signal inductive loads characterization up to 1.5 MHz and 7 kW," *IEEE Trans. Power Electron.*, vol. 23, no. 1, pp. 75–87, Jan. 2008.

[14] H. Sarnago, O. Lucia, and J. M. Burdio, "FPGA-based resonant load identification technique for flexible induction heating appliances," *IEEE Trans. Ind. Electron.*, vol. 65, no. 12, pp. 9421–9428, Dec. 2018.

[15] J. Villa, L. A. Barragan, J. I. Artigas, D. Navarro, A. Dominguez Vicente, and T. Cabeza, "SoC-based in-cycle load identification of induction heating appliances," *IEEE Trans. Ind. Electron.*, early access, Jul. 10, 2020, doi: 10.1109/TIE.2020.3007083.

[16] C. Franco, J. Acero, R. Alonso, C. Sagues, and D. Paesa, "Inductive sensor for temperature measurement in induction heating applications," *IEEE Sensors J.*, vol. 12, no. 5, pp. 996–1003, May 2012.

[17] J. Serrano, J. Acero, I. Lope, C. Carretero, J. M. Burdio, and R. Alonso, "Modeling of domestic induction heating systems with non-linear saturable loads," in *Proc. IEEE Appl. Power Electron. Conf. Expo. (APEC)*, Mar. 2017, pp. 3127–3133.

[18] O. Lucia, D. Navarro, P. Guillen, H. Sarnago, and S. Lucia, "Deep learning-based magnetic coupling detection for advanced induction heating appliances," *IEEE Access*, vol. 7, pp. 181668–181677, 2019.

[19] A. Bono-Nuez, C. Bernal-Ruíz, B. Martín-del-Brío, F. J. Pérez-Cebolla, and A. Martínez-Iturbe, "Recipient size estimation for induction heating home appliances based on artificial neural networks," *Neural Comput. Appl.*, vol. 28, no. 11, pp. 3197–3207, Nov. 2017. [Online]. Available: http://link.springer.com/10.1007/s00521-016-2227-6

[20] A. Bono-Nuez, B. Martin-del-Brio, C. Bernal-Ruiz, F. J. Perez-Cebolla, A. Martinez-Iturbe, and I. Sanz-Gorrachategui, "The inductor as a smart sensor for material identification in domestic induction cooking," *IEEE Sensors J.*, vol. 18, no. 6, pp. 2462–2470, Mar. 2018.

[21] Y. LeCun, Y. Bengio, and G. Hinton, "Deep learning," *Nature*, vol. 521, no. 7553, pp. 436–444, May 2015. [Online]. Available: http://www.nature.com/articles/nature14539

[22] R. C. Gonzalez, "Deep convolutional neural networks [Lecture Notes]," *IEEE Signal Process. Mag.*, vol. 35, no. 6, pp. 79–87, Nov. 2018.

[23] X. Tao, D. Zhang, Z. Wang, X. Liu, H. Zhang, and D. Xu, "Detection of power line insulator defects using aerial images analyzed with convolutional neural networks," *IEEE Trans. Syst., Man, Cybern. Syst.*, vol. 50, no. 4, pp. 1486–1498, Apr. 2020.

[24] A. H. Abdi, C. Luong, T. Tsang, G. Allan, S. Nouranian, J. Jue, D. Hawley, S. Fleming, K. Gin, J. Swift, R. Rohling, and P. Abolmaesumi, "Automatic quality assessment of echocardiograms using convolutional neural networks: Feasibility on the apical four-chamber view," *IEEE Trans. Med. Imag.*, vol. 36, no. 6, pp. 1221–1230, Jun. 2017.

[25] Y. Qian, M. Bi, T. Tan, and K. Yu, "Very deep convolutional neural networks for noise robust speech recognition," *IEEE/ACM Trans. Audio, Speech, Lang. Process.*, vol. 24, no. 12, pp. 2263–2276, Dec. 2016.
[26] G. Jiang, H. He, J. Yan, and P. Xie, "Multiscale convolutional neural networks for fault diagnosis of wind turbine gearbox," *IEEE Trans. Ind. Electron.*, vol. 66, no. 4, pp. 3196–3207, Apr. 2019.
[27] Z. Meng, X. Guo, Z. Pan, D. Sun, and S. Liu, "Data segmentation and augmentation methods based on raw data using deep neural networks approach for rotating machinery fault diagnosis," *IEEE Access*, vol. 7, pp. 79510–79522, 2019.
[28] J. Salamon and J. P. Bello, "Deep convolutional neural networks and data augmentation for environmental sound classification," *IEEE Signal Process. Lett.*, vol. 24, no. 3, pp. 279–283, Mar. 2017.

JORGE VILLA (Member, IEEE) received the M.Sc. degree in industrial engineering from the University of Zaragoza, Zaragoza, Spain, in 2016, where he is currently pursuing the Ph.D. degree in electronic engineering.

His main research interests include resonant converters and digital control for induction heating applications.

Mr. Villa is a member of the Aragon Institute for Engineering Research (I3A), Group of Power Electronics and Microelectronics (GEPM).

DENIS NAVARRO received the M.Sc. degree in microelectronics from the University of Montpellier, France, in 1987, and the Ph.D. degree from the University of Zaragoza, in 1992.

Since September 1988, he has been with the Department of Electronic Engineering and Communications, Universidad de Zaragoza, where he is currently a Professor. In 1993, he designed the first SPARC microprocessor in Europe. His current research interests include CAD for VLSI, low-power ASIC design, and modulation techniques for power converters. He is involved in the implementation of new applications of integrated circuits.

Dr. Navarro is a member of the Aragon Institute for Engineering Research (I3A).

ALBERTO DOMINGUEZ received the Ph.D. degree in electronic engineering from the University of Zaragoza, Spain, in 2017.

Since 2017, he has been working with BSH Home Appliances in the development of new domestic induction cooktops. His main research interests include modeling, control, and optimization of constrained systems, especially devoted to resonant inverters in domestic induction heating.

JOSE I. ARTIGAS received the M.Sc. and Ph.D. degrees in electrical engineering from the University of Zaragoza, Zaragoza, Spain, in 1989 and 1996, respectively.

He has been with the Department of Electronic Engineering and Communications, University of Zaragoza, where he is currently a Professor. He has been involved in different research and development projects. His main research interests include signal acquisition, digital control, and modulation strategies applied to power converters.

Dr. Artigas is a member of the Aragon Institute for Engineering Research (I3A), Group of Power Electronics and Microelectronics (GEPM).

LUIS A. BARRAGAN received the M.Sc. and Ph.D. degrees in physics from the University of Zaragoza, Zaragoza, Spain, in 1988 and 1993, respectively.

He is currently a Professor with the Department of Electronic Engineering and Communications, University of Zaragoza. He has been involved in different research and development projects on induction-heating systems for home appliances. His research interests include modeling and digital control applied to domestic induction heating.

Dr. Barragan is a member of the Aragon Institute for Engineering Research (I3A), Group of Power Electronics and Microelectronics (GEPM).